$D^*D\pi$ COUPLING CONSTANT IN 2 + 1 FLAVOR LATTICE QCD

A THESIS SUBMITTED TO
THE GRADUATE SCHOOL OF NATURAL AND APPLIED SCIENCES
OF
MIDDLE EAST TECHNICAL UNIVERSITY

BY

KADİR UTKU CAN

IN PARTIAL FULFILLMENT OF THE REQUIREMENTS
FOR
THE DEGREE OF MASTER OF SCIENCE
IN
PHYSICS

SEPTEMBER 2012

Approval of the thesis:

$D^*D\pi$ COUPLING CONSTANT IN 2 + 1 FLAVOR LATTICE QCD

submitted by **KADİR UTKU CAN** in partial fulfillment of the requirements for the degree of **Master of Science in Physics Department, Middle East Technical University** by,

Prof. Dr. Canan Özgen _____
Dean, Graduate School of **Natural and Applied Sciences**

Prof. Dr. Mehmet T. Zeyrek _____
Head of Department, **Physics**

Prof. Dr. Altuğ Özpineci _____
Supervisor, **Physics Department, METU**

Assoc. Prof. Dr. Güray Erkol _____
Co-supervisor, **Engineering Department, Özyeğin University**

Examining Committee Members:

Prof. Dr. Ali Ulvi Yılmazer
Ankara University, Physics Engineering Department _____

Prof. Dr. Altuğ Özpineci
Middle East Technical University, Physics Department _____

Assoc. Prof. Dr. Güray Erkol
Özyeğin University, Engineering Department _____

Assist. Prof. Dr. Hande Toffoli
Middle East Technical University, Physics Department _____

Assoc. Prof. Dr. Ismail Turan
Middle East Technical University, Physics Department _____

Date: _____

I hereby declare that all information in this document has been obtained and presented in accordance with academic rules and ethical conduct. I also declare that, as required by these rules and conduct, I have fully cited and referenced all material and results that are not original to this work.

Name, Last Name: KADİR UTKU CAN

Signature :

ABSTRACT

$D^*D\pi$ COUPLING CONSTANT IN 2 + 1 FLAVOR LATTICE QCD

Can, Kadir Utku
M.S., Department of Physics
Supervisor : Prof. Dr. Altuğ Özpineci
Co-Supervisor : Assoc. Prof. Dr. Güray Erkol

September 2012, 42 pages

Developments in high-performance computing instruments and advancements in the numerical algorithms combined with lattice gauge theory make it possible to simulate Quantum Chromodynamics (QCD), the theory of strongly-interacting quarks and gluons, numerically at nearly physical light-quark masses. In this work we present our results for the $D^*D\pi$ coupling constant as simulated on $32^3 \times 64$, unquenched 2 + 1-flavor lattices. We estimate the coupling at the chiral limit as $g_{D^*D\pi} = 16.23 \pm 1.71$, which is in good agreement with its experimental value $g^{(exp)}_{D^*D\pi} = 17.9 \pm 0.3 \pm 1.9$ as obtained by CLEO II Collaboration.

Keywords: Lattice QCD, Axial coupling, Axial current, D meson

ÖZ

$D^*D\pi$ ETKİLEŞİM SABİTİNİN ÖRGÜ KRD YÖNTEMİ İLE BELİRLENMESİ

Can, Kadir Utku
Yüksek Lisans, Fizik Bölümü
Tez Yöneticisi : Prof. Dr. Altuğ Özpineci
Ortak Tez Yöneticisi : Doç. Dr. Güray Erkol

Eylül 2012, 42 sayfa

Yüksek başarımlı hesaplama tekniklerindeki gelişmeler ile sayısal algoritmalar ve örgü ayar teorisindeki ilerlemeler sayesinde, kuvvetli etkileşen kuark ve gluonların teorisi olan Kuantum Renk Dinamiği (KRD) benzetişimlerinde neredeyse gerçek kuark kütlesini kullanmak mümkün olmuştur. Bu çalışmada deniz kuarklarının etkisi katılmış olan $32^3 \times 64$, 2 + 1-çeşnili örgüler kullanılarak $D^*D\pi$ etkileşim sabiti hesabı yapılmıştır. Gerçek kuark kütlesinde bulunan sonuç $g_{D^*D\pi} = 16.23 \pm 1.71$ olup, CLEO II deneyi tarafından belirlenen $g^{(exp)}_{D^*D\pi} = 17.9 \pm 0.3 \pm 1.9$ değeriyle uyumluluk göstermektedir.

Anahtar Kelimeler: Örgü KRD, Axial akım, D mezonu

to my dear family...

ACKNOWLEDGMENTS

I would like to thank my supervisor Assoc. Prof. Dr. Güray Erkol, without whom I won't be able to accomplish such a work. We have been more than a colleagues throughout this work. It has been a great honour to be his padawan and learn the ways of the *Force* (this is the highest ranking acknowledgement from me). I am also grateful to Prof. Dr. Altuğ Özpineci for his understanding, endless patience and will to transfer his knowledge to young generations. He, in the first place, is the one who educated me and motivated me to study in this field. Special thanks to Assist. Prof. Dr. Hande Toffoli for being such a great educator and helping me out to discover my aptness for programming. I also want to thank Prof. Dr. Ali Ulvi Yılmazer and Assoc. Prof. Dr. İsmail Turan for accepting to be a member of my jury. The sincerest thanks are for these wonderful five people for being so kind and supportive.

I would also like to thank two important people who had significant effect on my success. Thanks to Prof. Dr. Makoto Oka from Tokyo Institute of Technology for giving me the opportunity to visit Japan and for his wise guidance throughout my studies. Also thanks to Dr. Toru T. Takahashi from Gunma College of Technology for the educative and productive discussions that we had.

I want to thank Ece Aşılar for her tireless help and warmest thanks to Dr. Sinan Kuday for accepting me as a guest and for his friendship. Thanks to my fellow colleagues and friends Assist. Prof. Dr. Bora Işıldak, Kutlu Kutluer, Didem Çebi, Murat Metehan Türkoğlu, Ulaş Özdem, Taylan Takan, Dilege Gülmez, Vedat Tanrıverdi and all others who were present at my thesis defence, for all their support and best wishes. More thanks to my friends whose company I've always enjoyed whenever we met.

Finally, I want to thank my family, especially my mom, for their never-ending support and love. Thanks to them I am able to walk along this path with confidence. Thank you all.

All the numerical calculations in this work were performed on National Center for High Performence Computing of Turkey (Istanbul Technical University). The unquenched gauge configurations employed in our analysis were generated by PACS-CS collaboration [1]. We used

a modified version of Chroma software system [2]. This work was supported by The Scientific and Technological Research Council of Turkey (TUBITAK) under project number 110T245.

TABLE OF CONTENTS

LIST OF TABLES

TABLES

LIST OF FIGURES

FIGURES

CHAPTER 1

INTRODUCTION

We can describe the three of the four known forces with the Standard Model (SM) of the particle physics. This model constructs the theoretical foundations of the electromagnetic, weak and strong interactions of elementary particles and enables us to study the Nature in a systematic fashion. The SM is a gauge theory with the gauge group SU(3)×SU(2)×U(1) where the SU(2)×U(1) group constitutes the electroweak sector of the SM whereas the SU(3) is the gauge group of Quantum Chromo Dynamics (QCD) and governs the strong interactions. The elementary particles are classified as the Fermions and the Bosons. Fermion sector holds three families of quarks and leptons and their anti-particles with half-integer spins (e.g. $1/2$, $3/2$, ...), and the Boson sector has force carrying particles, the Gauge Bosons, with integer spins (e.g. 0, 1, ...). The quarks and gluons, apart from spin and charge quantum numbers like leptons and bosons, also carry a *color* quantum number, which leads to the strong interactions among them and the self-interactions of the gluons. One peculiarity of the strong interactions, or QCD, is the difference in the behaviour of the strong coupling constant α_s. Given in Figure 1.1, the α_s in the high energy limit decreases so that the quarks and gluons nearly don't interact among themselves as $Q \to \infty$. This behaviour is known as the *asymptotic freedom* and we are able to do perturbative calculations in the high-energy regime since the α_s is small enough. Although we have been able to observe the leptons and bosons, not a single quark or gluon is observed yet. It is believed that the color-interaction potential between the quarks and gluons is responsible for this peculiar phenomena in such a way that the quarks, anti-quarks and gluons are *confined* to the colorless objects: *hadrons*, a plentiful of which have been observed. Hadrons are classified according to their quark content as *baryons* and *mesons* where the baryons are formed by three (anti-)quarks and mesons consists of a quark anti-quark pair. Investigating hadrons gives us an insight into their internal structure

(electric charge, spin distributions etc.), helps us to identify the non-perturbative QCD effects on the experimental observables (*i.e.* CKM matrix elements [6]) and predict the parameters related to their decays [7]. However, due to the non-linear running of the strong-coupling constant, α_s, perturbation theory breaks down at small momentum transfers since the coupling constant becomes large (see Figure 1.1) and has a Landau Pole at the typical QCD scale, $\Lambda_{QCD} \approx 200$ MeV, where it diverges. In this low-energy regime (*i.e.*, at energy scale $Q^2 \leq 1$ GeV^2), where the hadrons live, non-perturbative methods are necessary.

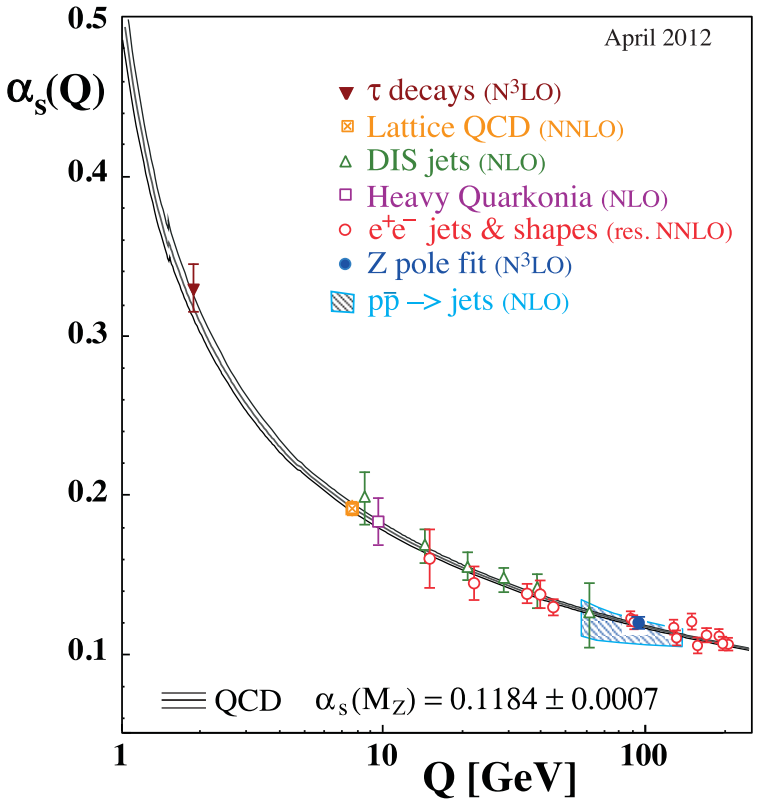

Figure 1.1: Running of the strong coupling constant, α_s, [3].

In order to probe the hadron structure and extract the information theoretically, non-perturbative methods have been developed such as the QCD Sum Rules (QCDSR) [8] or the Chiral Perturbation Theory (χPT). While each method has proven itself to be successful, it would be rather naive to think that they are flawless. Considering the QCDSR for example, results may have uncontrollable uncertainties due to several reasons: The condensates which describe the non-perturbative nature of the QCD vacuum or in the case of Light Cone QCDSR errors that arise from the distribution amplitudes can introduce some uncertainty. In addition, the continuum part of the spectrum describing the excited states or the Borel stability region which indicates

the independence to the unphysical *Borel-Mass parameter* may be misidentified. Despite these uncertainties QCDSR provide us very valuable information regarding the hadronic observables (see [9, 10] and references therein). χPT [11, 12] on the other hand, is an effective field theory formulated as a perturbative expansion over m_π and contains the coupling constants as input parameters which have to be fitted to the experimental data or calculated from other theoretical methods.

One other promising non-perturbative method is Lattice QCD (LQCD). It is an *ab initio* method starting directly from the QCD Lagrangian which simulates the strong interactions numerically on a discretized Euclidean space-time. LQCD method has proven itself over years and has become even more reliable with technological and algorithmic advancements in the last years. Some of its remarkable achievements are the precise spectroscopy measurements [1] and the prediction for the behavior of the running coupling constant [4] (see Figure 1.2) consistent with the experiments. Lattice community actively studies the hadronic observables to gain a better perspective on the hadron structure and interactions, as well as to provide valuable input to other methods [13].

These non-perturbative methods have been applied to light ($u,\ d,\ s$) and heavy ($c,\ b$) quark sectors extensively but the charm sector still requires more attention from LQCD. Charm physics plays a significant role in understanding the quark-gluon plasma, a new phase of the QCD matter where quarks and gluons are believed to live as free particles. The suppression of the charmonium state J/ψ is considered as a signal for the formation of this new phase. It is possible that J/ψ can be absorbed by light mesons (*i.e.* π, ρ) or nucleons (see ref. [14]) abundant in the later stages of the heavy ion collisions like the ones in RHIC or LHC's Pb-Pb collisions. Below are some possible absorption reactions that may occur.

$$\pi + J/\psi \to D + \bar{D}^*, \quad \bar{D} + D^*$$
$$\rho + J/\psi \to D + \bar{D}$$
$$N + J/\psi \to \Lambda_c + D$$

We see that specific coupling constants at the hadronic vertices (*e.g.* $g_{D^*D\pi}$ etc.) are needed to give an accurate description of charm-hadron production and suppression in collisions performed at RHIC.

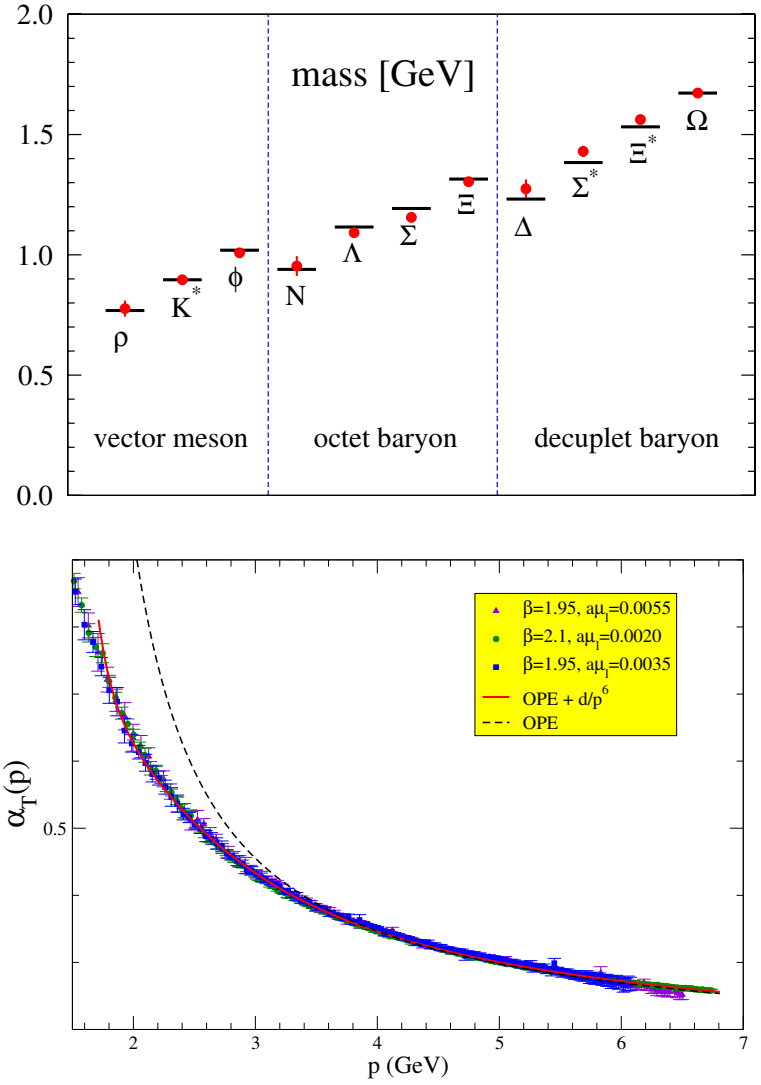

Figure 1.2: Remarkable Lattice QCD results: Hadron spectroscopy (up) and running coupling constant (down), compare with Figure 1.1. Plots are from Ref. [1] and [4] respectively.

In this work we concentrate on one particular hadronic observable: The $D^*D\pi$ coupling constant, $g_{D^*D\pi}$. The reason we choose this coupling is primarily because there is enough phase space for $D^* \to D\pi$ decay and it is possible to compare our result to experimental data obtained from CLEO II experiment [15].

There are several results available in the literature estimated by both QCDSR and LQCD. QCDSR calculations, however, underestimate the $D^*D\pi$ coupling constant(e.g. $g^{(QCDSR)}_{D^*D\pi} = 9 \pm 2$ or $g^{(LCQCDSR))}_{D^*D\pi} = 11 \pm 2$. See Ref. [16]) compared to its experimental value, $g^{(exp)}_{D^*D\pi} = 17.9 \pm 0.3 \pm 1.9$. An earlier LQCD result [17] on the other hand is in good agreement with experiment, $g^{(lqcd)}_{D^*D\pi} = 18.8 \pm 2.3^{+1.1}_{-2.0}$. This lattice result was obtained on $24^3 \times 64$ quenched

(sea-quark effects ignored) lattices. We estimate our results from simulations on $32^3 \times 64$ unquenched (with sea-quark effects), $2+1$-flavor (u, d, s) lattices and with a different simulation method than used in Ref. [17].

This thesis is organized as follows. In Chapter 2 we discuss the Lattice-QCD method by demonstrating how to discretize the space-time and continuum action and sketch the typical workflow. The method we use and the simulation details are given in Chapter 3. We present our results and discuss the possible source of errors in Chapter 4. Conclusions are summarized in Chapter 5.

CHAPTER 2

LATTICE QCD

Like any other renormalizable quantum field theory, QCD needs an ultraviolet regularization if we want to extract physical information. Discretizing the space-time to a *lattice* introduces an intrinsic momentum cut-off proportional to the inverse of the lattice spacing "a" and provides a regularization *per se*. In addition to regularization, we should also consider how to quantize our theory. Euclidean path-integral formalism governs the quantization of the lattice theory and is the main instrument to calculate the physical observables. Correlation functions give access to the observables, namely the hadronic properties such as the energy of the hadron or the matrix elements:

$$\lim_{T\to\infty} \langle \hat{O}_2(t)\hat{O}_1(0)\rangle_T = \sum_h \langle 0|\hat{O}_2|h\rangle\langle h|\hat{O}_1|0\rangle e^{-E_h t} \tag{2.1}$$

and in the path-integral formalism we can write,

$$\langle \hat{O}_2(t)\hat{O}_1(0)\rangle = \frac{1}{Z_T}\int \mathcal{D}[\Psi] e^{-S_E[\Psi]} O_2[\Psi(\vec{x},t)] O_1[\Psi(\vec{x},0)] \tag{2.2}$$

where $\hat{O}_2(t)$, $\hat{O}_1(0)$ are the Euclidean operators, E_h is the energy of the intermediate hadronic state, Z_T is the partition function, $Z_T = \int \mathcal{D}[\Psi] e^{-S_E[\Psi]}$, and S_E is the Euclidean action. The hadron operators $\hat{O}_1$ and $\hat{O}_2$ create(annihilate) the hadronic states with the quantum numbers that they carry, which in turn creates(annihilates) not only the ground state but also the excited states of the hadron in question. The limit description in Eq. (2.1) ensures that, as the time evolves only the ground state survives.

The choice of Euclidean space-time holds the key to solve the theory numerically. It is real-

ized by a *Wick rotation* to imaginary time and Eq. (2.2) shows two notable benefits of such $t \rightarrow -it$ transformation: i) This *rotation* clearly reveals the resemblance between the statistical and quantum field theories, enabling the use of statistical methods such as Monte Carlo integration, where the e^{-S_E} term is interpreted as the weight factor. ii) In contrast to the Minkowski version the wildly oscillating exponent is now an exponential decay, e^{-S_E}, changing the integral to a well-behaved function.

The path integral formalism is suitable to solve with Monte Carlo integration on a finite lattice, however the underlying theory should also be discretized like the lattice itself. The following sections cover the *naive discretization of fermions*, Wilson Gauge action and the improved discretized actions used in this work.

2.1 Discrete Space-time and QCD

Throughout this section, we follow the Gattringer & Lang's [18] notation.

2.1.1 Discrete Space-time

The first thing to do is to replace the continuum space-time with the discrete 4D lattice. Let's denote it by Λ:

$$\Lambda = \Big\{ n = (n_1,\ n_2,\ n_3,\ n_4),\ |\ n_{1,2,3} = 0, 1, \ldots, N-1, \\ n_4 = 0, 1, \ldots, N_T - 1 \Big\}, \tag{2.3}$$

where N_T is the total number of the time steps and N is the total number of the spatial steps. We impose the condition that the fermion fields are restricted to the lattice sites and allowed to move step by step on straight lines only,

$$\psi(\mathbf{x}) \rightarrow a^{-3/2}\, \psi(a\mathbf{n}), \qquad \bar{\psi}(\mathbf{x}) \rightarrow a^{-3/2}\, \bar{\psi}(a\mathbf{n}), \tag{2.4}$$

where $\mathbf{n}$ is the coordinate vector $(\vec{n}, n_4)$ and "a" is the lattice spacing, which we drop for simplicity.

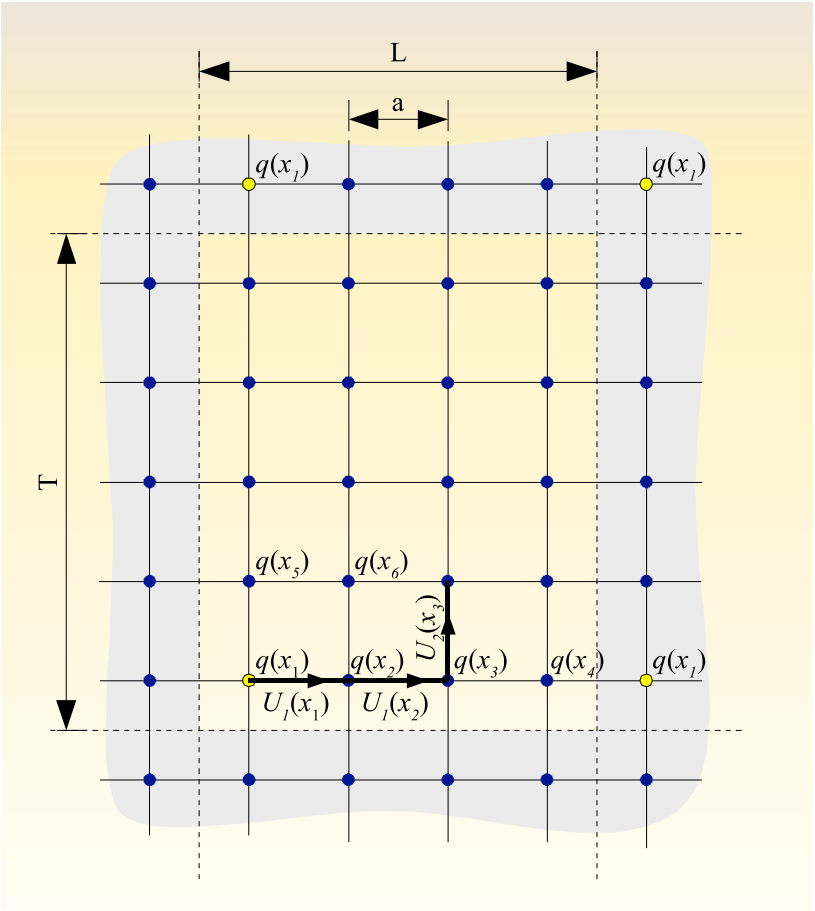

Figure 2.1: A 2D slice of a periodic lattice with fermion fields and *Link Variables*. [5]

The gauge fields of the continuum theory are replaced by the so-called *Link Variables* U_μ, which are the connections between the lattice sites. Technically speaking, they are the elements of the $SU(3)_c$ group with each matrix element corresponding to the probability density of transition from one color component to another,

$$U_\mu = \begin{array}{c} \\ r \\ g \\ b \end{array} \begin{array}{c} \begin{array}{ccc} r & g & b \end{array} \\ \begin{pmatrix} U_\mu^{rr} & U_\mu^{rg} & U_\mu^{rb} \\ U_\mu^{gr} & U_\mu^{gg} & U_\mu^{gb} \\ U_\mu^{br} & U_\mu^{bg} & U_\mu^{bb} \end{pmatrix} \end{array} \tag{2.5}$$

Link variables are related to the continuum fields by an exponent;

$$U_\mu(n) = exp\ (iaA_\mu(n)). \tag{2.6}$$

Shrinking the infinite space-time to a finite hypercube raises the question about the nature

of the boundaries, whether the lattice should have periodic or anti-periodic boundary conditions. For our purposes we choose periodic boundary conditions to conserve the discrete translational symmetry.

$$\begin{aligned} \psi(0,n_2,n_3,n_4) &= \psi(N,n_2,n_3,n_4) \qquad & U_\mu(N,n_2,n_3,n_4) &= U_\mu(0,n_2,n_3,n_4) \\ &\vdots & &\vdots \\ \psi(n_1,n_2,n_3,0) &= \psi(n_1,n_2,n_3,N_T) & U_\mu(n_1,n_2,n_3,N_T) &= U_\mu(n_1,n_2,n_3,0) \end{aligned} \tag{2.7}$$

Now we have discretized the main components, all we need to do is to reformulate our theory accordingly.

2.1.2 Discrete QCD

The familiar continuum QCD action is as follows:

$$S[\psi,\bar{\psi},A] = \sum_{f=1}^{N_f} \int d^4x\, \bar{\psi}^{(f)}(x)_{\alpha c}[\not{\partial} + ig\not{A}(x) + m^{(f)}]\psi^{(f)}(x)_{\alpha c} + \frac{1}{2}\int d^4x\, Tr[F_{\mu\nu}F^{\mu\nu}] \tag{2.8}$$

where $\psi^{(f)}(x)_{\alpha c}$, $\bar{\psi}^{(f)}(x)_{\alpha c}$ are the fermion, anti-fermion spinors with Dirac, flavor and color indices α, f and c, respectively. A_μ is the gauge field, g is the strong coupling constant and $F_{\mu\nu}$ is the field strength tensor,

$$F_{\mu\nu} = \partial_\mu A_\nu(x) - \partial_\nu A_\mu(x) + ig[A_\mu, A_\nu]. \tag{2.9}$$

Taking the color components of the gauge fields into account,

$$A_\mu(x) = \sum_{i=1}^{8} A^i_\mu(x) T_i \ , \tag{2.10}$$

we can rewrite Eq. (2.9) as,

$$F_{\mu\nu}(x) = \sum_{i=1}^{8} \left\{ \partial_\mu A^i_\nu(x) - \partial_\nu A^i_\mu(x) - g f_{jki} A^j_\mu A^k_\nu \right\} T_i \tag{2.11}$$

and denoting,

$$F^i_{\mu\nu}(x) = \partial_\mu A^i_\nu(x) - \partial_\nu A^i_\mu(x) - g f_{jki} A^j_\mu A^k_\nu \tag{2.12}$$

with T_i being the Gell-Mann matrices and f_{jki} the structure constant of the SU(3) group, we can rewrite the QCD action as,

$$S[\psi, \bar{\psi}, A] = \sum_{f=1}^{N_f} \int d^4x \, \bar{\psi}^{(f)}(x)_{\alpha c} [\not{\partial} + ig\not{A}(x) + m^{(f)}] \psi^{(f)}(x)_{\alpha c} - \frac{1}{4} \sum_{i=1}^{8} \int d^4x F^i_{\mu\nu}(x) F^{\mu\nu}_i(x) \tag{2.13}$$

where the repeated indices are summed over as usual but we have indicated explicitly that there are eight observable color combinations for gluons.

Before we start discretizing QCD, there are some important issues to mention, since we switched to the Euclidean metric. First, the change of Dirac index convention from $\mu = 0, 1, 2, 3 \equiv (t, x, y, z)$ to $\mu = 1, 2, 3, 4 \equiv (x, y, z, t)$ and secondly the use of chiral basis gamma matrices,

$$\gamma_1 = -i\gamma_1^M, \quad \gamma_2 = -i\gamma_2^M, \quad \gamma_3 = -i\gamma_3^M, \quad \gamma_4 = \gamma_0^M$$
$$\left\{\gamma_\mu, \gamma_\nu\right\} = 2\delta_{\mu\nu}\mathbb{1}$$

where the $\gamma^M_{0,1,2,3}$ matrices are the usual Minkowski ones.

In order to simplify the discussion let's consider the fermionic and gluonic parts of the action separately.

2.1.3 Fermion Action

In addition to the aforementioned discretizations, we shall use the central-difference discretization for the partial derivative,

$$\partial_\mu \psi(\mathbf{n}) = \frac{\psi(\mathbf{n} + \hat{\mu}) - \psi(\mathbf{n} - \hat{\mu})}{2a}. \tag{2.14}$$

where $\hat{\mu}$ is the unit vector in the μ direction. We also replace the integral over all space by a sum over all lattice points.

Starting from the Dirac equation form, the discretized action is,

$$S_F[\psi,\bar{\psi}] = a^4 \sum_{\mathbf{n}\in\Lambda} \bar{\psi}(\mathbf{n}) \left[\sum_{\mu=1}^{4} \gamma_\mu \frac{\psi(\mathbf{n}+\hat{\mu}) - \psi(\mathbf{n}-\hat{\mu})}{2a} + m\psi(\mathbf{n}) \right] \tag{2.15}$$

However it is easy to see that this action is not gauge-invariant under SU(3) gauge transformations of the form,

$$\psi(n) \to \psi'(n) = \Omega(n)\psi(n) \qquad \bar{\psi}(n) \to \bar{\psi}'(n) = \bar{\psi}(n)\Omega^\dagger(n) \tag{2.16}$$

where $\Omega(n)$ is an SU(3) phase.

This is the same problem as the continuum case which in return had led us to a redefinition of the partial derivative as a covariant derivative. Following the footsteps, we are going to do the same trick, but with different terminology. Defining the gauge transformation of link variables as,

$$U_\mu(n) \to U'_\mu(n) = \Omega(n) U_\mu(n) \Omega^\dagger(n+\hat{\mu}), \tag{2.17}$$

we can use them like the comparator [19] of the continuum theory and construct an SU(3) gauge-invariant fermion action.

$$S_F[\psi,\bar{\psi},U] = a^4 \sum_{\mathbf{n}\in\Lambda} \bar{\psi}(\mathbf{n}) \left[\sum_{\mu=1}^{4} \gamma_\mu \frac{U_\mu(\mathbf{n})\psi(\mathbf{n}+\hat{\mu}) - U_\mu^\dagger(\mathbf{n}-\hat{\mu})\psi(\mathbf{n}-\hat{\mu})}{2a} + m\psi(\mathbf{n}) \right] \tag{2.18}$$

The discretization scheme we have covered is called the *naive discretization of fermions*. Of course one should show that in the continuum limit Eq. (2.18) reduces to the continuum action. When we use the Taylor expansions,

$$U_\mu(\mathbf{n}) = 1 + iaA_\mu(\mathbf{n}) + O(a^2) \tag{2.19a}$$

$$U_\mu^\dagger(\mathbf{n}-\hat{\nu}) = 1 - iaA_\mu(\mathbf{n}-\hat{\mu}) + O(a^2) \tag{2.19b}$$

$$A_\mu(\mathbf{n}-\hat{\mu}) = A_\mu(\mathbf{n}) + O(a) \tag{2.19c}$$

$$\psi(\mathbf{n}\pm a) = \psi(\mathbf{n}) + O(a) \tag{2.19d}$$

we recover the continuum action up to $O(a)$,

$$S_F[\psi, \bar{\psi}, U] = a^4 \sum_{\mathbf{n}\in\Lambda} \sum_{\mu=1}^{4} \bar{\psi}(\mathbf{n}) \left(\gamma_\mu \partial_\mu + m\right) \psi(\mathbf{n}) + i a^4 \sum_{\mathbf{n}\in\Lambda} \sum_{\mu=1}^{4} \bar{\psi}(\mathbf{n}) \gamma_\mu A_\mu(\mathbf{n}) \psi(\mathbf{n}) + O(a). \quad (2.20)$$

Note that the sum over all lattice points introduces a term proportional to $1/a^4$, thus the first two terms are of the order of zero with respect to a.

2.1.4 Gauge Action

The gauge action discretization is rather straightforward and follows from the fact that we need a locally gauge-invariant object. The only component we have to use is the link variables shown in Figure 2.2.

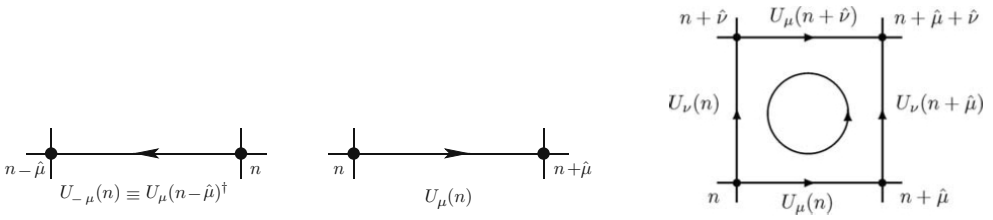

Figure 2.2: Forward and backward link variables (left) and 1×1 Plaquette $U_{\mu\nu}$, constructed from four link variables (right).

Following the geometrical origin of the $F_{\mu\nu}$ we construct the most basic gauge-invariant object with them, the so-called *Plaquette*, shown in Figure 2.2.

$$U_{\mu\nu}(n) = U_\mu(n) U_\nu(n+\hat{\mu}) U_\mu^\dagger(n+\hat{\nu}) U_\nu^\dagger(n) \quad (2.21)$$

Using the plaquette definition we can write the *Wilson gauge action* as,

$$S_G[U] = \frac{\beta}{3} \sum_{n\in\Lambda} \sum_{\mu<\nu} Re\left\{Tr[\mathbb{1} - U_{\mu\nu}(n)]\right\}, \quad (2.22)$$

where β is the lattice coupling and it is inversely proportional to the strong coupling, $\beta = 6/g^2$.

We can show that in the $a \to 0$ limit, this action approximates the continuum one up to $O(a^2)$. Using Eqs. (2.19a), (2.19b) and the Baker-Campbell-Hausdorff formula for the product of exponentials of matrices:

$$\exp(A)\exp(B) = \exp\left(A + B + \frac{1}{2}[A, B] + \dots\right), \tag{2.23}$$

we expand the plaquette,

$$U_{\mu\nu} = \exp(iaA_\mu(n) + iaA_\nu(n+\hat{\mu}) - \frac{a^2}{2}[A\mu(n), A_\nu(n+\hat{\mu})]) \tag{2.24}$$

$$- iaA_\mu(n+\hat{\nu}) - iaA_\nu(n) - \frac{a^2}{2}[A\mu(n+\hat{\nu}), A_\nu(n)]) \tag{2.25}$$

$$+ \frac{a^2}{2}[A\nu(n+\hat{\mu}), A_\mu(n+\hat{\mu})]) + \frac{a^2}{2}[A\mu(n), A_\nu(n)]) \tag{2.26}$$

$$+ \frac{a^2}{2}[A\mu(n), A_\mu(n+\hat{\nu})] + \frac{a^2}{2}[A\nu(n+\hat{\mu}), A_\nu(n)]) + O(a^3)) \tag{2.27}$$

and Taylor expanding the resulting fields $A_\mu(n+\hat{\mu}) = A_\mu(n) + a\partial_\mu A_\mu + O(a^2)$, further simplifies the plaquette expression,

$$U_{\mu\nu} = \exp(ia^2(\partial_\mu A_\nu(n) - \partial_\nu A_\mu + i[A_\mu(n), A_\nu(n)]) + O(a^3)) \tag{2.28}$$

$$= \exp(ia^2 F_{\mu\nu}(n) + O(a^3)), \tag{2.29}$$

and we see that action reduces to,

$$S_G[U] = \frac{\beta}{3}\sum_{n\in\Lambda}\sum_{\mu<\nu} Re\left\{Tr[\mathbb{1} - U_{\mu\nu}(n)]\right\} = \frac{a^4}{2g^2}\sum_{n\in\Lambda}\sum_{\mu<\nu} Tr\left[F_{\mu\nu}(n)^2\right] + O(a^2). \tag{2.30}$$

This discrete formulation of QCD was first done by Kenneth G. Wilson in his 1974 paper [20]. His formulation indeed showed that the physical information can be extracted from first-principles calculations. However, in the contrary it led to other discretization-related problems. We have mentioned the discretization errors in sections 2.1.3 and 2.1.4, when we said that discrete actions approximate the continuum ones up to order $O(a)$ and $O(a^2)$ respectively. Even though one thinks that when we take the continuum limit $a \to 0$, these errors would go to zero; practically, simulating an $a = 0$ lattice is impossible for numerical calculations and these errors will always be counted as systematical errors. Thus, corrections

are necessary to improve the discretization errors and to better approximate the continuum actions. One should keep in mind of course that these correction terms should vanish in the continuum limit. Iwasaki gauge action [21], Lüscher-Weisz gauge action [22], the non-perturbatively $O(a)$-improved Wilson fermion action, or also known as the clover action [23] are some improved actions.

Apart from discretization errors there is also another important problem with the naive discretization which is the *Fermion Doubling*. We will deal with this problem in the following section in the context of our choice of improved fermion action and we will see that we adapt our solution in the price of explicitly breaking the chiral symmetry. There are other solutions that take chiral symmetry into account such as the overlap fermions [24] and related domain-wall fermions [25], staggered fermions [26] and twisted-mass fermions [27] which are out of the scope of this thesis.

2.1.5 Fermion Doubling and Wilson Term

Fermion Doubling arises in the naive discretization when we consider the quark propagator, which is necessary to calculate the correlation functions. To explicitly see the doubling problem let's identify the Dirac term from Eq. (2.18) as below and invert it.

$$D(n|m) = \sum_{\mu=1}^{4} \gamma_\mu \frac{U_\mu(n)\delta_{n+\hat{\mu},m} - U_\mu^\dagger(n)\delta_{n-\hat{\mu},m}}{2a} + m\,\delta_{n,m}. \tag{2.31}$$

Here, we have dropped the flavor, Dirac and color indices and let's consider a trivial gauge configuration $U_\mu = \mathbb{1}$ for simplicity. Using,

$$\delta_{n,m} = \frac{1}{|\Lambda|} \sum_{k_\mu} e^{-iak_\mu(\mathbf{n}-\mathbf{m})}, \tag{2.32}$$

where $|\Lambda| = N^3 N_T$ is the total number of lattice sites, we can Fourier transform the Dirac operator,

$$\tilde{D}(n|m) = \frac{1}{|\Lambda|} \sum_{n,m\in\Lambda} \sum_{\mu=1}^{4} \gamma_\mu \frac{e^{-iak_\mu(\mathbf{n}+\hat{\mu}-\mathbf{m})} - e^{-iak_\mu(\mathbf{n}-\hat{\mu}-\mathbf{m})}}{2a} + m\, e^{-iak_\mu(\mathbf{n}-\mathbf{m})} \tag{2.33}$$

by factoring out $e^{-iak_\mu(\mathbf{n}-\mathbf{m})}$ and using Eq. (2.32), we get,

$$\tilde{D}(n|m) = \delta_{n,m}\left(\frac{i}{a}\sum_{\mu=1}^{4} sin(k_\mu a)\gamma_\mu + m\mathbb{1}\right), \tag{2.34}$$

where we have also used the Euler's formula for the *sine* function and dropped the unit vector $|\hat{\mu}| = 1$. Defining the term in parenthesis as $D(k)$ and multiplying the Eq. (2.34) with $D(k)^{-1}$ from right we find the relation,

$$\tilde{D}(n|m)D(k)^{-1} = \delta_{n,m} \tag{2.35}$$

which tells us to compute the inverse of the $D(k)$,

$$D(k)^{-1} = \frac{m\mathbb{1} - ia^{-1}\sum_\mu sin(k_\mu a)\gamma_\mu}{m^2 + a^{-2}\sum_\mu sin^2(k_\mu a)} \tag{2.36}$$

and inverse Fourier transform to get the quark propagator $D(n|m)^{-1}$,

$$D(n|m)^{-1} = \frac{1}{|\Lambda|}\sum_{k\in\tilde{\Lambda}} D^{-1}(k)e^{-iak(n-m)} \tag{2.37}$$

The *fermion-doubling* problem is evident when we analyze Eq. (2.36). To simplify the discussion further, lets consider massless fermions and concentrate on the denominator term which has a pole for $k = (0, 0, 0, 0)$ corresponding to physical fermions.

$$D(k)^{-1} = \frac{-ia^{-1}\sum_\mu sin(k_\mu a)\gamma_\mu}{a^{-2}\sum_\mu sin^2(k_\mu a)} \tag{2.38}$$

However, due to the periodicity of the sine function it is easy to see that $k = (\pi/a, 0, 0, 0)$, $(0, \pi/a, 0, 0)$, $\ldots$, $(\pi/a, \pi/a, \pi/a, \pi/a)$, values all give rise to in total $2^d - 1$ unphysical fermions, the so-called *doublers*.

The solution to this problem suggested by Wilson (1975) is to add a term to the fermion action such that the Fourier transformed Dirac operator becomes,

$$\tilde{D}(k) = m\mathbb{1} + \frac{i}{a}\sum_{\mu=1}^{4} sin(k_\mu a)\gamma_\mu + \mathbb{1}\frac{1}{a}\sum_{\mu=1}^{4}\Big(1 - cos(k_\mu a)\Big). \tag{2.39}$$

The relevant term turns out to be the 4D lattice Laplace operator,

$$-\frac{a}{2}\hat{\Box} = -a\sum_{\mu=1}^{4}\frac{U_\mu(n)\delta_{n+\hat{\mu},m} - 2\delta_{n,m} + U_\mu^\dagger(n)\delta_{n-\hat{\mu},m}}{2a^2} \tag{2.40}$$

where the constant a ensures that the *Wilson term* vanishes as $a \to 0$. We can write the corrected Dirac operator as,

$$D(n|m) = \left(m + \frac{4}{a}\right)\delta_{n,m} - \frac{1}{2a}\sum_{\mu=1}^{4}\Big[\Big(\mathbb{1} + \gamma_\mu\Big)U_\mu(n)\delta_{n+\hat{\mu},m} + \Big(\mathbb{1} - \gamma_\mu\Big)U_\mu^\dagger(n)\delta_{n-\hat{\mu},m}\Big] \tag{2.41}$$

and the doubler-free Wilson fermion action becomes,

$$S_F^W[\psi, \bar{\psi}, U] = a^4 \sum_{\mathbf{n},\mathbf{m}\in\Lambda} \bar{\psi}(n)D(n|m)\psi(m). \tag{2.42}$$

As mentioned before, the $4/a$ factor introduced by the *Wilson term* explicitly breaks the chiral symmetry which in turn forces us to perform chiral extrapolations.

For future discussions we will do a factorization of the Dirac term and introduce the *hopping parameter* κ, which is an important lattice parameter:

$$\begin{aligned} D(n|m) &= C(\mathbb{1} - \kappa H(n|m)), \quad \kappa = \frac{1}{2(ma+4)}, \quad C = m + \frac{4}{a} \\ H(n|m) &= \sum_{\mu=1}^{4}\Big[\Big(\mathbb{1} + \gamma_\mu\Big)U_\mu(n)\delta_{n+\hat{\mu},m} + \Big(\mathbb{1} - \gamma_\mu\Big)U_\mu^\dagger(n)\delta_{n-\hat{\mu},m}\Big]. \end{aligned} \tag{2.43}$$

2.1.6 Improved Actions

One should control the systematical errors due to discretization in order to obtain more reliable results. This is best done by improving the actions to have smaller discretization errors. We showed in subsequent sections that naive fermion and gauge actions have $O(a)$ and $O(a^2)$ discretization errors respectively. It is common sense to use actions that have same discretization errors. We now briefly discuss the improved actions used in this work.

2.1.6.1 Iwasaki Gauge Action

Since we do not generate lattices but instead use the ones generated by PACS-CS collaboration, we are not directly involved in the choice of gauge action; so we refer to the related paper for details [1] and references therein. Here we briefly discuss the Iwasaki action. PACS-CS use the plaquette-only Wilson gauge action by adding a rectangular loop term [28] like shown in Figure 2.3. The action is given by,

$$S_G = \frac{\beta}{6}\left\{c_0 \sum_{x,\mu<\nu} W^{1\times1}_{\mu\nu}(x) + c_1 \sum_{x,\mu<\nu} W^{1\times2}_{\mu\nu}(x)\right\} \tag{2.44}$$

where the coefficient of the rectangular loop $W^{1\times2}_{\mu\nu}(x)$, $c_1 = -0.331$, is fixed by an approximate renormalization group analysis [21]. The normalization condition, $c_0 + 8c_1 = 1$, can be obtained following the procedure in Section 2.1.4, where the coefficient of the c_1 term is fixed so that the Iwasaki action reduces to the continuum action in the $a \to 0$ limit. Using this condition, the coefficient of the plaquette $W^{1\times1}_{\mu\nu}(x)$, is found to be $c_0 = 1 - 8c_1 = 3.648$.

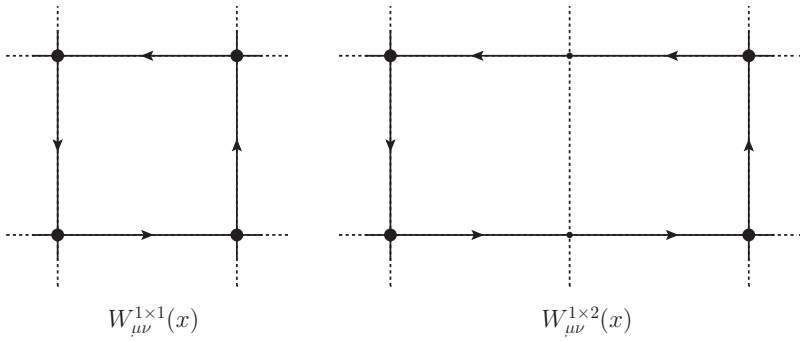

Figure 2.3: Plaquette and rectangular loop contributions to Iwasaki action

2.1.6.2 Clover Fermion Action

For the sake of consistency with PACS-CS lattices, we choose the clover action to calculate our valence quark propagators. Clover action is a non-perurbatively $O(a)$ improved version of the Wilson action in Eq. (2.42) according to the *Symanzik improvement program* [22]. The action is written as [23],

$$S^C_F = S^W_F + \kappa_q\, c_{SW}\, a^5 \sum_{n\in\Lambda}\sum_{\mu<\nu} \bar{\psi}(n)\frac{1}{2}\sigma_{\mu\nu}F_{\mu\nu}(n)\psi(n) \tag{2.45}$$

where *Sheikholeslami-Wohlert* term is found to be $c_{SW} = 1.715$ [29], $\sigma_{\mu\nu} = \frac{1}{2}[\gamma_\mu, \gamma_\nu]$, κ_q is the hopping parameter of the quark and $F_{\mu\nu}(n)$ is discretized as the difference of the sum of the plaquettes like shown in Figure 2.4,

$$F_{\mu\nu}(n) = \frac{1}{8i}\left(Q_{\mu\nu}(n) - Q^{\dagger}_{\mu\nu}(n)\right) \tag{2.46}$$

$$Q_{\mu\nu}(n) = U_{\mu,\nu}(n) + U_{\nu,-\mu}(n) + U_{-\mu,-\nu}(n) + U_{-\nu,\mu}(n) \tag{2.47}$$

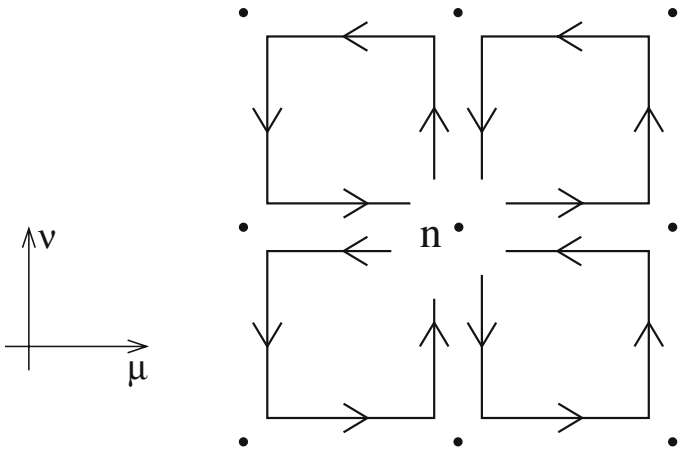

Figure 2.4: Sum of plaquettes in the μ-ν plane. Compare with Eq. (2.21) and Figure 2.2.

2.2 Workflow

The idea is to compute the correlation functions and when doing so we need quark propagators calculated on each individual gauge configuration or lattice. To make things more clear lets consider such a two-point correlation function,

$$\begin{aligned}\left\langle O_M(n)\bar{O}_M(m)\right\rangle = -\frac{1}{\mathcal{Z}}\int \mathcal{D}[U]e^{-S_G[U]}\,\det[D_u]\,\det[D_d]\,\det[D_s] \\ \times\; Tr\left[\Gamma\, D^{-1}_{q_1}(n|m)\,\Gamma\, D^{-1}_{q_2}(m|n)\right] \\ \mathcal{Z} = \int \mathcal{D}[U]e^{-S_G[U]}\det[D_u]\,\det[D_d]\,\det[D_s],\end{aligned} \tag{2.48}$$

where $O_M(n)$ and $\bar{O}_M(m)$ are a generic meson's annihilation, creation operators defined as $O_M(n) = \bar{q_1}(n)\Gamma q_2(n)$ and $\bar{O}_M(m) = \bar{q_2}(m)\bar{\Gamma}q_1(m)$, respectively. Determinants $\det[D_u]$, $\det[D_d]$ and $\det[D_s]$ are obtained after integrating out the fermion action and the trace term comes

form the quark field contractions according to the Wick's Theorem. The Γ is a combination of γ-matrices specific to the meson M.

There are two independent steps in calculating such correlation functions. First one is the Monte Carlo generation of the lattice according to the "$e^{-S_G[U]} \det[D_u] \det[D_d] \det[D_s]$" term which acts like the Boltzman factor and includes the sea-quark effects via the fermion determinants. Lattice generation is out of the scope of this work and we refer the interested reader to the Gattringer and Lang's book [18], which has a nice introductory chapter on generating gauge configurations. Further techniques related to the configurations used in this work can be found at the PACS-CS paper [1].

The second step is the computation of the quark propagators $D_f^{-1}(n|m)$, on each gauge configuration for each flavor f and contract them to find the value of the correlation function. When this procedure is repeated sufficiently many times one can approximate the integral according to the importance sampling,

$$\langle O \rangle = \lim_{N\to\infty} \frac{1}{N} \sum_{n=1}^{N} O[U_n] \tag{2.49}$$

where $O[U_n]$ stands for the value of the function on each gauge configuration.

Ideally, one should calculate such propagators from each site on the lattice for each quark flavor that forms the hadron, which is extremely time and resource consuming considering the inversion of the Dirac operator matrix and the high statistical needs. As a workaround one chooses a *source* point and computes the propagator from that point to all other lattice sites:

$$D^{-1}(n|m_0) = \sum_{\alpha,a} D^{-1}(n|m)_{\substack{\beta\alpha \\ ba}} S(m)_{\substack{\alpha \\ a}} \tag{2.50}$$

A typical choice for the source is a Dirac delta function which, in turn called as a *point source*.

$$S(m)_{\substack{\alpha \\ a}} = \delta(m - m_0)\delta_{\alpha\alpha_0}\delta_{aa_0} \tag{2.51}$$

where the α and a are the Dirac and color indices. However, if one wants to improve the ground-state dominance (*i.e.* ground-state saturation after fewer time steps), then the *smeared sources* are favored:

$$S(m) = \sum_{i}^{N} \delta(m - m_0) e^{\sigma \nabla^2} \tag{2.52}$$

$$\nabla^2 = \sum_{j=1}^{3} \Big(U_j(\mathbf{n}, n_t)\delta(\mathbf{n} + \hat{j}, m) + U_j^{\dagger}(\mathbf{n} - \hat{j}, n_t)\delta(\mathbf{n} - \hat{j}, n_t) \Big) \tag{2.53}$$

where N is the number of smearing steps applied to the Dirac delta function and σ is a constant, dimensionless *smearing parameter*. The set of values for N and σ are chosen so that the resulting hadron's root mean square radius is around 1 fm. This type of smearing is known as *gauge-invariant-gaussian smearing* or shortly, *shell smearing*. As a special case, choosing $\sigma = 0$ and summing over all lattice sites leads to *wall smearing*, which improves ground state dominance but suffers from large statistical errors.

CHAPTER 3

METHOD

3.1 Theory

In order to extract the vector-pseudoscalar-pion coupling constant $g_{VP\pi}$, we should calculate the $\langle P(p')|A^{\mu}(q)|V(p,\lambda)\rangle$ transition matrix element. This matrix element can be parameterized with three form factors [17]:

$$\begin{aligned}\langle P(p')|A^{\mu}(q)|V(p,\lambda)\rangle = 2m_V F_0(q^2)\frac{\epsilon^{\lambda}.q}{q^2}q^{\mu} \\ + (m_P + m_V)F_1(q^2)[\epsilon^{\lambda\mu} - \frac{\epsilon^{\lambda}.q}{q^2}q^{\mu}] \\ + F_2(q^2)\frac{\epsilon^{\lambda}.q}{m_P + m_V}[p^{\mu} + p^{'\mu} - \frac{m_V^2 - m_P^2}{q^2}q^{\mu}],\end{aligned} \tag{3.1}$$

where $F_0(q^2)$, $F_1(q^2)$ and $F_2(q^2)$ are the form factors, ϵ^{λ} is the polarization of the vector meson and the transferred momentum is given by, $q^{\mu} = (p - p')^{\mu}$.

PCAC relation [30, 31] and meson-dominance model [32], implies that the divergence of the axial-vector current $q_{\mu}A^{\mu}$ is dominated by a soft pion:

$$\langle P(p')|q^{\mu}A^{\mu}(q)|V(p,\lambda)\rangle = g_{VP\pi}\frac{\epsilon^{\lambda}(p).q}{m_{\pi}^2 - q^2}f_{\pi}m_{\pi}^2 + \dots \tag{3.2}$$

Comparing Eq. (3.1) and Eq. (3.2) it is straightforward to identify the coupling in the zero momentum transfer as

$$g_{VP\pi} = \frac{2m_V F_0(0)}{f_{\pi}}, \tag{3.3}$$

where f_π is the pion decay constant.

Further investigation of Eq.(3.1) reveals that the first term, which contains F_0 form factor, has a pole at $q^2 = 0$ due to $1/q^2$ factor. So, an indirect approach is necessary to extract $F_0(0)$. Regrouping the terms containing $\frac{\epsilon^\lambda.q}{q^2}q^\mu$ factor, we get,

$$\begin{aligned}\langle P(p')|A^\mu(q)|V(p,\lambda)\rangle &= (m_P + m_V)F_1(q^2)\epsilon^{\lambda\mu} \\ &+ (p'^\mu + p^\mu)F_2(q^2)\frac{\epsilon^\lambda.q}{m_P + m_V} \\ &+ \frac{\epsilon^\lambda.q}{q^2}q^\mu\left[2m_V F_0(q^2) - (m_P + m_V)F_1(q^2) - (m_V - m_P)F_2(q^2)\right].\end{aligned} \tag{3.4}$$

Note the the square-bracketed term should be zero in the $q^2 = 0$ limit to regulate the last term. Exploiting this requisite we factorize the $F_0(q^2)$ form factor in terms of $F_1(q^2)$ and $F_2(q^2)$,

$$2m_V F_0(q^2) = (m_P + m_V)F_1(q^2) + (m_V - m_P)F_2(q^2) \tag{3.5}$$

leading Eq.(3.3) to

$$g_{VP\pi} = \frac{1}{f_\pi}\left[(m_P + m_V)F_1(0) + (m_V - m_P)F_2(0)\right]. \tag{3.6}$$

Defining,

$$G_1(q^2) = \frac{m_V + m_P}{f_\pi}F_1(q^2) \quad , \quad G_2(q^2) = \frac{m_V - m_P}{f_\pi}F_2(q^2) \tag{3.7}$$

and rearranging the Eq. (3.6) reveals the dominant contribution of $G_1(0)$ to coupling,

$$g_{VP\pi} = G_1(0)\left(1 + \frac{G_2(0)}{G_1(0)}\right) \tag{3.8}$$

Having reduced the problem to the determination of those two form factors we note that it is possible to calculate $G_1(0)$ directly but $G_2(0)/G_1(0)$ vanishes at $q^2 = 0$ due to G_2's q dependence, so its value should be extrapolated to $q^2 = 0$.

3.2 Correlation Functions and Ratios

The matrix elements, hence the form factors, can be isolated by forming the appropriate ratios of the three- and two-point correlations functions having the form,

$$C^{(3)bc}_{\mu\nu}(t_x, \vec{q}; t_y, \vec{p}) = \sum_{\vec{x},\vec{y}} e^{-i\vec{q}.\vec{x}} e^{-i\vec{p}.\vec{y}} \left\langle P^c(y) A^\nu(x) V^b_\mu(0) \right\rangle \tag{3.9}$$

$$C^{(2)bb}_{PP}(t_y; \vec{p}) = \sum_{\vec{y}} e^{-i\vec{p}.\vec{y}} \left\langle P^b(y) P^b(0) \right\rangle \tag{3.10}$$

$$C^{(2)cc}_{V_\mu V_\nu}(t_y; \vec{p}) = \sum_{\vec{y}} e^{-i\vec{p}.\vec{y}} \left\langle V^c_\mu(y) V^c_\nu(0) \right\rangle \tag{3.11}$$

where $P \equiv \bar{q}'\gamma_5 q$ and $V \equiv \bar{q}'\gamma_\mu q$ are pseudoscalar and vector-meson interpolating fields , b and c are generic smearing labels and t_x and t_y are the current insertion's and sink operator's time slices, respectively.

To extract the $q^2 = 0$ matrix element and relate it to the $G_1(0)$, we should study the following ratio (see Appendix A for details),

$$R_1(t) = \frac{C^{(3)SW}_{ii}(t)\sqrt{Z_V}\sqrt{Z_P}}{C^{(2)SS}_{V_iV_i}(t) C^{(2)WW}_{PP}(t_y - t)} \sqrt{V} \tag{3.12}$$

S and W denote that the meson operators are shell- and wall-smeared and $\sqrt{V}$ is to cover for the volume factor that arises due to different smearing choices. Figure 3.1 illustrates the Feynman diagram of the Eq. (3.12).

The normalization factors Z_V and Z_P are obtained from exponential fits to the two-point correlators,

$$C^{(2)}_{PP}(t; \vec{p}) \simeq Z_P \frac{e^{-E_P t}}{2E_P}, \qquad C^{(2)}_{V_\mu V_\nu}(t; \vec{p}) \simeq Z_V \frac{e^{-E_V t}}{2E_V}(\delta_{\mu\nu} - \frac{p_\mu p_\nu}{p^2}), \tag{3.13}$$

where E_P and E_V are ground state energies of the mesons.

As stated before the $G_2(0)/G_1(0)$ term should be obtained via extrapolation of momentum injected matrix elements which can be accessed after some cumbersome combination of the ratios,

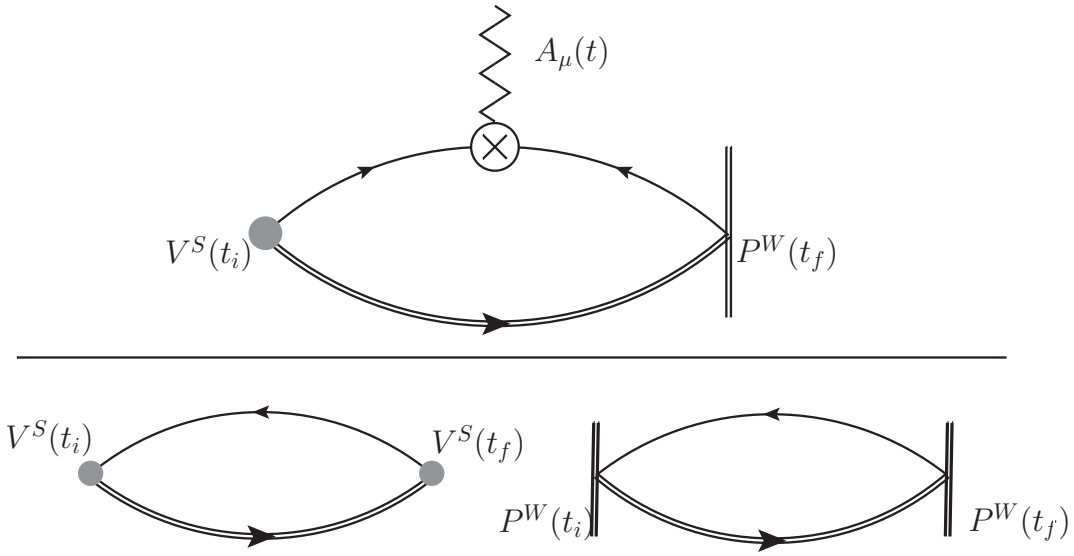

Figure 3.1: Feynman diagram of $R_1(t)$. Curved double lines indicate the heavy quark, grey dots are the shell smeared sources and vertical double lines are the wall smeared sinks.

$$R_2(t) = \frac{C_{10}^{(3)SW}(t,\vec{q})\sqrt{Z_V}\sqrt{Z_P}}{C_{V_2V_2}^{(2)SS}(t,\vec{q})C_{PP}^{(2)WW}(t_y-t)}\sqrt{V}, \tag{3.14}$$

$$R_3(t) = \frac{C_{11}^{(3)SW}(t,\vec{q})\sqrt{Z_V}\sqrt{Z_P}}{C_{V_2V_2}^{(2)SS}(t,\vec{q})C_{PP}^{(2)WW}(t_y-t)}\sqrt{V}, \tag{3.15}$$

$$R_4(t) = \frac{C_{22}^{(3)SW}(t,\vec{q})\sqrt{Z_V}\sqrt{Z_P}}{C_{V_2V_2}^{(2)SS}(t,\vec{q})C_{PP}^{(2)WW}(t_y-t)}\sqrt{V}, \tag{3.16}$$

Form factors F_1 and F_2 are related to the ratios as such,

$$F_1(\vec{q}=0,\ t) = \frac{R_1(t)}{m_V+m_P}, \qquad F_1\left(\vec{q}=\frac{2\pi}{L}(q_x,q_y,q_z),\ t\right) = \frac{R_4(t)}{m_V+m_P} \tag{3.17}$$

$$\frac{F_2}{F_1}(t) = \frac{(m_V+m_P)^2}{2m_P^2\vec{q}^{\,2}}\left[\left(\vec{q}^{\,2}-E_V(E_V-m_P)\right)+\frac{m_V(E_V-m_P)}{E_V}\frac{R_3(t)}{R_4(t)}+i\frac{m_V^2 q_1}{E_V}\frac{R_2(t)}{R_4(t)}\right], \tag{3.18}$$

One expects the F_2/F_1 ratio to be insensitive to the changes of transferred momentum around the pion pole since both form factors have the same pole and are far away from the next pole, which is the axial vector meson a_1.

3.3 Axial-Vector Current Renormalization

The axial-vector current has to be renormalized in order to match the lattice results to their continuum counterparts. We follow the one-loop perturbative method in the modified minimal subtraction ($\overline{MS}$) scheme described in the App.C of the CP-PACS paper [33]. The renormalized current is

$$A_\mu^R = u_0 Z_A \left(1 + b_A \frac{m_q}{u_0}\right) A_\mu, \tag{3.19}$$

where $A_\mu = \bar{q}\gamma_\mu\gamma_5 q$ is the bare local current and m_q is the valence quark mass determined from the relation,

$$m_q = \frac{1}{2}\left(\frac{1}{\kappa_q} - \frac{1}{\kappa_{critical}}\right), \tag{3.20}$$

where $\kappa_{critical}$ is the value producing zero quark mass.

The constants Z_A and b_A depend on the running coupling constant,

$$Z_A = 1 - 0.0215 g^2_{\overline{MS}}(\mu) \tag{3.21}$$

$$b_A = 1 + 0.0378 g^2_{\overline{MS}}(\mu) \tag{3.22}$$

and u_0 is

$$u_0 = P^{1/4} = \left(1 - \frac{0.8412}{\beta}\right), \tag{3.23}$$

where P is the expectation value of the plaquette and β is the lattice coupling.

3.4 Simulation Details

We carry out our simulations on $32^3 \times 64$, $\beta = 1.9$, $2 + 1$ flavor PACS-CS lattices [1] generated with the non-perturbatively $O(a)$-improved Wilson quark action (sea quarks) and

Iwasaki gauge action. The lattice spacing is $a = 0.0907(13)$fm ($a^{-1} = 2.176(31)$GeV). We compute the u,d and c quark propagators with the same action as the sea quarks . We use $\kappa_{ud} = 0.13700, 0.13727, 0.13754, 0.13770$ and $\kappa_c = 0.1224$ for light and heavy-quark propagators respectively. The κ_{ud} values are chosen to be consistent with the sea quark κ_{ud}^{sea} of the configurations and we have fixed the value of κ_c so as to produce the charmonium mass. The hopping parameter of the strange quark present in the sea is fixed to $\kappa_s^{sea} = 0.1364$.

We create a vector meson D^* on site $\mathbf{n} = (\vec{0}, 0)$ using shell-smeared operator to improve the ground-state dominance. As the time evolves D^* interacts with an axial-vector current at an arbitrary time between the $t = [0, 12]$ interval. Then the meson is annihilated after 12 time steps, on the sink point $\mathbf{n} = (\vec{0}, 0)$, as a pseudo-scalar D-meson. To overcome the difficulties of the sequential-source method [34] (*i.e.* either fixing the insertion current or the source/sink momentum) we implement the *wall-smearing* method (see Appendix B), in which we applied wall smearing to the D-meson annihilation operator. However, one should note that the wall-sink smearing simplifies the computation in exchange of higher statistical fluctuations, making it hard to identify the fit region of *wall-wall* two point correlation functions. Also one caveat is that, the wall-smearing method, unlike the shell smearing, is not gauge-invariant; hence a specific gauge must be chosen, which leads to increased computation time or resources. In our case, we fix the gauge configurations to Coulomb gauge.

The meson interpolating-field operators are,

$$D(x) = \bar{d}(x)\gamma_\mu c(x), \qquad D(x) = \bar{d}(x)\gamma_5 c(x) \tag{3.24}$$

and we shell-(wall-) smear the $D^*(D)$ operators according to the Eqs. (3.12),(3.14),(3.15),(3.16) smearing labels. Investigating the three-point interaction shown in Figure 3.1, we see that the interacting propagator line is broken and hence in addition to the forward u, d and c propagators calculated from $\mathbf{n} = (\vec{0}, 0)$, one more backward u, d propagator is necessary. In order to calculate the backward propagator one should choose a source and we fix its source as $\mathbf{n} = (\vec{0}, 12)$ as imposed by the sink point. Individual forward *ud*, forward c and backward *ud* propagators are computed on 45, 50, 90 and 70 configurations for $\kappa_{ud} = 0.13700,\ 0.13727,\ 0.13754$ and 0.13770 respectively.

Propagator computation is followed by the contraction procedure to obtain the two- and three-

point correlation functions. Two-point correlators are calculated with respect to the three-point functions' smearing labels.

CHAPTER 4

RESULTS

Appropriate ratios of the correlation functions tend to stay constant as time evolves and ground state dominates. This constant behaviour is identified as *plateau regions* in the plots drawn with respect to time (see e.g. Figure 4.1). Effective mass plots in Figure 4.1 shows identified regions for two point correlation functions and Table 4.1 summarises our fits in that regions.

Table 4.1: Vector and pseudo scalar meson's normalization constants and ground-state energies. 45, 50, 90 and 70 data sets are used to fit Z_V and Z_P whereas the $a\ m_{D^*}$ and $a\ m_D$ are extracted from 36, 50, 50 and 70 data sets on κ_{ud} = 0.13700, 0.13727, 0.13754, 0.13770 lattices respectively.

κ_{ud}	Z_V	Z_P	$a\ m_{D^*}$	$a\ m_D$
0.13700	2.051×10^{-12}	4.013×10^{8}	1.011(7)	0.943(6)
0.13727	1.965×10^{-12}	4.341×10^{8}	0.979(7)	0.922(4)
0.13754	1.643×10^{-12}	5.153×10^{8}	0.972(7)	0.901(5)
0.13770	1.426×10^{-12}	4.466×10^{8}	0.938(9)	0.888(8)

The normalization factors Z_V and Z_P are obtained from *shell-shell* and *wall-wall* two-point correlators respectively, while the ground-state energies are fitted to *shell-point* correlators.

We find that the G_2/G_1 contributes to the coupling $\approx 1\%$. Our values are listed in Table 4.2 and fit regions are given in Figure 4.2 and Figure 4.3.

Table 4.2: Dominant and minor contributions to the coupling $g_{D^*D\pi}$.

κ_{ud}	$G_1(q^2 = 0)$	G_2/G_1	$g_{D^*D\pi}$
0.13700	14.15 ± 1.58	0.09(2)	15.45 ± 1.78
0.13727	13.63 ± 1.57	0.12(4)	15.24 ± 1.81
0.13754	12.76 ± 1.43	0.15(7)	15.54 ± 2.08
0.13770	15.46 ± 2.17	0.07(6)	16.44 ± 2.41

4.1 Chiral Extrapolations

As we stated before, technical drawbacks force us to carry our simulations with unphysical quark masses on lattices. In order to estimate the $g_{D^*D\pi}$ at the physical point we extrapolate our results to the chiral point (*i.e.* $m_q \to 0$).

- **Linear fit**: We fit our data to the function,

$$g_{D^*D\pi} = a_1 + a_2(a\, m_\pi)^2 \tag{4.1}$$

  from which it is possible to fix the values $a_{1,2}$. We can then extract the coupling constant by choosing the physical m_π value.

- **Quadratic fit**: We also fit to a quadratic function of the form,

$$g_{D^*D\pi} = b_1 + b_2(a\, m_\pi)^2 + b_3(a\, m_\pi)^4 \tag{4.2}$$

The linear and quadratic fit results are given in Table 4.3 and illustrated in Figure 4.4.

Table 4.3: Extrapolated values of $g_{D^*D\pi}$. Errors are estimated from 45 samples.

χ-fit	linear	quadratic	exp.
$g_{D^*D\pi}$	16.23 ± 1.71	17.09 ± 3.23	17.9 ± 2.2

4.2 Discussion of Errors

There may be several sources of systematical errors affecting our results. We can categorize these sources as:

- **Discretization errors**: The aptness of the Clover action may be questioned for heavy quarks since it has discretization errors $O(a\, m_Q)$ but it is rather vacillating to consider the *charm* as a heavy quark like the *bottom*. In order to predict such systematical errors, simulations should be repeated with lattices having different lattice spacings, a, and the consistency between the final results should be checked. However, in our current work we simulated our results with only one lattice spacing (a = 0.0907 fm) and thus we are unable to study the effect of the discretization.

- **Finite-volume effects**: These lattice artefacts are caused since we model the infinite space-time as a finite-size hypercube. In principle, finite volume effects are negligible as long as $m_\pi L > 4$. Considering we have $m_\pi L$ in the range $4.5 \leq m_\pi L \leq 10$ we assume minimal effect. However it is dependent on the object that is created on the lattice and one should check the effects of the finite volume by re-simulating the calculations on different sized lattices. Since we have $32^3 \times 64$ lattices only we can not estimate the finite size effects but the analysis in Ref. [17] suggests 6% of error for lattices smaller than ours. We may expect to have less errors than they found but we won't be reflecting this error to our final results.

- **Renormalization**: We estimate the axial-vector current renormalization constant in a perturbative way as mentioned in Section 3.3. Comparing to the approach for vector-current renormalization [33] and estimated error of $O(10)\%$ in Ref. [35] we can expect to have approximately same errors.

- **Chiral extrapolation**: We ignore the fit errors on parameters $a_{1,2}$ and $b_{1,2,3}$ since we expect negligible errors compared to the overall statistical error. Regarding the smaller errors, we choose to consider the linear extrapolation value as our result.

Apart from systematical errors there are also statistical errors related to the Monte Carlo sampling of the observables or fitting to data. In order to estimate these errors we employ the jackknife resampling method.

CHAPTER 5

CONCLUSION

In our work we have estimated the $D^*D\pi$ coupling constant by employing the ab initio Lattice QCD method.

Throughout the thesis we have discussed the discretization of the continuum QCD and introduced the *lattice* theory relevant to this work in a naive and rather compact fashion. Establishing the theoretical foundations we have outlined the typical workflow and difficulties of the numerical calculations. We have also studied the parameterization of the transition matrix element, $\langle P(p')|A^\mu|V(p,\lambda)\rangle$, in order to extract the coupling from the matrix element calculated by the proper combinations of the correlation functions computed on lattice. We performed our simulations on $32^3 \times 64$ sized lattices with lattice spacing $a = 0.0907(13)$ fm ($a^{-1} = 2.176(31)$GeV) and $2+1$ flavor dynamical quarks. The coupling is determined on four different gauge configurations with $\kappa_{ud}^{(sea)} = (0.13700, 0.13727, 0.13754, 0.13770)$ which correspond to $m_\pi \sim (700, 570, 410, 300)$ MeV and with physical strange quark, $\kappa_s^{(sea)} = 0.1364$.

We estimate the pionic coupling of the ground state D-mesons, $g_{D^*D\pi}$, as,

$$g_{D^*D\pi} = 16.23 \pm 1.71 \qquad g_{D^*D\pi}^{(exp)} = 17.9 \pm 0.3 \pm 1.9$$

which is in good agreement with the experiment. Our value is larger compared to the several QCD Sum Rules results and consistent with the previous lattice estimation.

More precise measurements may be desirable but regarding the $> 10\%$ experimental error, next logical step would be to estimate the systematical errors in a more subtle manner by re-performing the simulations on different sized lattices or by computing the quark propagators with improved Fermilab action [36], which is an improved version of the Clover action. Considering the resources we have however, it is not possible to estimate the systematical errors

in the near future; instead generalizing this study to extract the axial-vector form factors and studying the vector form factors of the D-mesons would be more feasible.

REFERENCES

[1] S. Aoki, K.-I. Ishikawa, N. Ishizuka, T. Izubuchi, D. Kadoh, K. Kanaya, Y. Kuramashi, Y. Namekawa, M. Okawa, Y. Taniguchi, A. Ukawa, N. Ukita, and T. Yoshié, "2+1 flavor lattice QCD toward the physical point," *Phys. Rev. D*, vol. 79, p. 034503, Feb 2009.

[2] R. G. Edwards and B. Joo, "The Chroma software system for lattice QCD," *Nucl.Phys.Proc.Suppl.*, vol. 140, p. 832, 2005.

[3] J. B. et al., "Review of Particle Physics," *Phys. Rev. D*, vol. 86, p. 010001, 2012.

[4] B. Blossier, P. Boucaud, M. Brinet, F. De Soto, X. Du, *et al.*, "The Strong running coupling at τ and Z_0 mass scales from lattice QCD," 2012.

[5] W. Wolfram, "Low energy QCD and physics of hadrons," Technische Universtat München, Presented at the SNP School 2012 at Japan, 2010.

[6] M. Okamoto, "Full determination of the CKM matrix using recent results from lattice QCD," *PoS*, vol. LAT2005, p. 013, 2006.

[7] D. Drechsel and T. Walcher, "Hadron structure at low Q^2," *Rev. Mod. Phys.*, vol. 80, pp. 731–785, Jul 2008.

[8] M. A. Shifman, A. Vainshtein, and V. I. Zakharov, "QCD and Resonance Physics. Sum Rules," *Nucl.Phys.*, vol. B147, pp. 385–447, 1979.

[9] B. L. Ioffe, "QCD at Low Energies," *Prog.Part.Nucl.Phys.*, vol. 56, pp. 232–277, 2006.

[10] L. Reinders, H. Rubinstein, and S. Yazaki, "Hadron properties from QCD sum rules," *Physics Reports*, vol. 127, no. 1, pp. 1 – 97, 1985.

[11] J. Gasser and H. Leutwyler, "Chiral Perturbation Theory: Expansions in the Mass of the Strange Quark," *Nucl.Phys.*, vol. B250, p. 465, 1985.

[12] S. Weinberg, "Phenomenological Lagrangians," *Physica*, vol. A96, p. 327, 1979.

[13] Ph. Hagler, "Hadron structure from lattice quantum chromodynamics," *Physics Reports*, vol. 490, no. 3-5, pp. 49 – 175, 2010.

[14] S. G. Matinyan and B. Muller, "A Model of charmonium absorption by light mesons," *Phys.Rev.*, vol. C58, pp. 2994–2997, 1998.

[15] S. Ahmed *et al.*, "First measurement of Gamma(D*+)," *Phys.Rev.Lett.*, vol. 87, p. 251801, 2001.

[16] F. Duraes, F. Navarra, M. Nielsen, and M. Robilotta, "Meson loops and the g(D*D pi) coupling," *Braz.J.Phys.*, vol. 36, pp. 1232–1237, 2006.

[17] A. Abada, D. Becirevic, P. Boucaud, G. Herdoiza, J. Leroy, *et al.*, "First lattice QCD estimate of the $g_{D^*D\pi}$ coupling," *Phys.Rev.*, vol. D66, no. 074504, 2002.

[18] C. Gattringer and C. B. Lang, *Quantum chromodynamics on the lattice*, vol. 788. 2010.

[19] M. E. Peskin and D. V. Schroeder, *An Introduction To Quantum Field Theory (Frontiers in Physics)*. Westview Press, 1995.

[20] K. G. Wilson, "Confinement of quarks," *Phys. Rev. D*, vol. 10, pp. 2445–2459, Oct 1974.

[21] Y. Iwasaki, "Renormalization Group Analysis of Lattice Theories and Improved Lattice Action. II four-dimensional non-abelian SU(N) gauge model," *UTHEP-118 (unpublished)*, 1983.

[22] M. Luscher and P. Weisz, "On-Shell Improved Lattice Gauge Theories," *Commun.Math.Phys.*, vol. 97, p. 59, 1985.

[23] B. Sheikholeslami and R. Wohlert, "Improved Continuum Limit Lattice Action for QCD with Wilson Fermions," *Nucl.Phys.*, vol. B259, p. 572, 1985.

[24] H. Neuberger, "Exactly massless quarks on the lattice," *Phys.Lett.*, vol. B417, pp. 141–144, 1998.

[25] D. B. Kaplan, "A Method for simulating chiral fermions on the lattice," *Phys.Lett.*, vol. B288, pp. 342–347, 1992.

[26] J. B. Kogut and L. Susskind, "Hamiltonian Formulation of Wilson's Lattice Gauge Theories," *Phys.Rev.*, vol. D11, p. 395, 1975.

[27] R. Frezzotti, S. Sint, and P. Weisz, "O(a) improved twisted mass lattice QCD," *JHEP*, vol. 0107, p. 048, 2001.

[28] S. Aoki *et al.*, "Comparative study of full QCD hadron spectrum and static quark potential with improved actions," *Phys.Rev.*, vol. D60, p. 114508, 1999.

[29] S. Aoki *et al.*, "Nonperturbative O(a) improvement of the Wilson quark action with the RG-improved gauge action using the Schrodinger functional method," *Phys.Rev.*, vol. D73, p. 034501, 2006.

[30] M. Gell-Mann and M. Levy, "The axial vector current in beta decay," *Nuovo Cim.*, vol. 16, p. 705, 1960.

[31] Y. Nambu, "Axial Vector Current Conservation in Weak Interactions," *Phys. Rev. Lett.*, vol. 4, pp. 380–382, Apr 1960.

[32] J. J. Sakurai, *Currents and mesons*. Chicago: University of Chicago Press, 1969.

[33] A. Ali Khan, S. Aoki, G. Boyd, R. Burkhalter, S. Ejiri, M. Fukugita, S. Hashimoto, N. Ishizuka, Y. Iwasaki, K. Kanaya, T. Kaneko, Y. Kuramashi, T. Manke, K. Nagai, M. Okawa, H. P. Shanahan, A. Ukawa, and T. Yoshié, "Light hadron spectroscopy with two flavors of dynamical quarks on the lattice," *Phys. Rev. D*, vol. 65, p. 054505, Feb 2002.

[34] W. Wilcox, T. Draper, and K.-F. Liu, "Chiral limit of nucleon lattice electromagnetic form factors," *Phys. Rev. D*, vol. 46, pp. 1109–1122, Aug 1992.

[35] G. Erkol, M. Oka, and T. T. Takahashi, "Axial Charges of Octet Baryons in Two-flavor Lattice QCD," *Phys.Lett.*, vol. B686, pp. 36–40, 2010.

[36] M. B. Oktay and A. S. Kronfeld, "New lattice action for heavy quarks," *Phys.Rev.*, vol. D78, p. 014504, 2008.

APPENDIX A

Ratio

Let's consider the ratio given in Eq. (3.12),

$$R(t) = \frac{C^{(3)}_{ii}(t)\,\sqrt{Z_V}\,\sqrt{Z_P}}{C^{(2)}_{V_iV_i}(t)C^{(2)}_{PP}(t_y - t)} \tag{A.1}$$

The operators in Euclidean correlators are written in Heisenberg picture and to investigate this ratio lets write it again in Schrödinger picture. From simple quantum mechanics we know that operators in Heisenberg and Schrödinger picture are related as,

$$\left\langle \hat{O}(t) \right\rangle_H = \left\langle e^{Ht}\ \hat{O}\ e^{-Ht} \right\rangle_S \tag{A.2}$$

remembering that the imaginary factor i is dropped due to Wick rotation, $t \to -it$.

Converting the correlation functions to Schrödinger picture we get,

$$C^{(3)}_{\mu\nu}(t_y, t_x; t) = \sum_{P,V_\mu} \left\langle 0|e^{Ht_y}\ \hat{P}\ e^{-Ht_y}|P\right\rangle \left\langle P|e^{Ht}\ A_\nu\ e^{-Ht}|V\right\rangle \left\langle V|e^{Ht_x}\ \hat{V}_\mu\ e^{-Ht_x}|V_\mu\right\rangle \Big|_{t_x=0} \tag{A.3}$$

$$\underset{a << t < t_y}{=} e^{-E_P(t_y-t)}e^{-E_{V_\mu}t} \left\langle 0|\hat{P}|P\right\rangle \left\langle P|\hat{A}_\nu|V_\mu\right\rangle \left\langle V_\mu|\hat{V}_\mu|0\right\rangle \tag{A.4}$$

$$C^{(2)}_{PP}(t_y, t_x) = \sum_{P} \left\langle 0|e^{Ht_y}\ \hat{P}\ e^{-Ht_y}|P\right\rangle \left\langle P|e^{-Ht_x}\ \hat{P}\ e^{-Ht_x}|0\right\rangle \Big|_{t_x=0} \tag{A.5}$$

$$\underset{a << t < t_y}{=} e^{-E_Pt} \left|\left\langle 0|\hat{P}|P\right\rangle\right|^2 \tag{A.6}$$

$$C^{(2)}_{V_\mu V_\mu}(t_y, t_x) = \sum_{V_\mu} \left\langle 0|e^{Ht}\ \hat{V}_\mu\ e^{-Ht}|V_\mu\right\rangle \left\langle V_\mu|e^{Ht_x}\ \hat{V}_\mu\ e^{-Ht_x}|0\right\rangle \Big|_{t_x=0} \tag{A.7}$$

$$\underset{a << t < t_y}{=} e^{-E_{V_\mu}t} \left|\left\langle 0|\hat{V}_\mu|V_\mu\right\rangle\right|^2 \tag{A.8}$$

where we can identify the $Z_P = \left|\left\langle 0|\hat{P}|P\right\rangle\right|^2$ and $Z_V = \left|\left\langle 0|\hat{V}_\mu|V_\mu\right\rangle\right|^2$ from Eq. (3.13)

By putting Z_P, Z_V and Eqs. (A.4), (A.6), (A.8) into the Eq. (A.1) we see that it reduces to the coupling,

$$R = \left\langle P|\hat{A}_\nu|V_\mu\right\rangle = g_{VPA_\mu} \tag{A.9}$$

APPENDIX B

Wall-Smearing Method

The three point correlation function can be written in terms of the quark propagators $S(x, x')$ after the contractions specified by *Wick's Theorem*,

$$\langle C^{D^* A_\mu D}(t_2, t_1; \mathbf{p}', \mathbf{p})\rangle = -i \sum_{\mathbf{x_2},\mathbf{x_1}} e^{-i\mathbf{p}\cdot\mathbf{x_2}} e^{i\mathbf{q}\cdot\mathbf{x_1}} \langle \mathrm{Tr}[\gamma_\mu \, S_u(0, x_1) \, \gamma_\mu\gamma_5 \, S_u(x_1, x_2) \, \gamma_5 \, S_c(x_2, 0)]\rangle \tag{B.1}$$

While point-to-all propagators $S_u(0, x_1)$ and $S_c(x_2, 0)$ can be easily obtained, the computation of all-to-all propagator $S_u(x_1, x_2)$ is a formidable task. One common method is to use a *sequential source* composed of $S_u(0, x_1)$ and $S_c(x_2, 0)$ for the Dirac matrix and invert it in order to compute $S_u(x_1, x_2)$ [34]. However, this method requires to fix either the inserted current or the sink momentum.

An approach that does not require to fix any of the above is the *wall-smearing method*, where a summation over the spatial sites at the sink time point, $\mathbf{x_2}$, is made before the inversion. This corresponds to having a wall source or sink:

$$\langle C_{SW}^{D^* A_\mu D}(t_2, t_1; \mathbf{0}, \mathbf{p})\rangle = -i \sum_{\mathbf{x_2},\mathbf{x_2'},\mathbf{x_1}} e^{i\mathbf{q}\cdot\mathbf{x_1}} \langle \mathrm{Tr}[\gamma_\mu \, S_u(0, x_1) \, \gamma_\mu\gamma_5 \, S_u(x_1, x_2') \, \gamma_5 \, S_c(x_2, 0)]\rangle \tag{B.2}$$

where the propagator (instead of the hadron state) is projected on to definite momentum (S and W are smearing labels for *shell* and *wall*). The wall method has the advantage that one can first compute the shell and wall propagators and then contract these to obtain the three-point correlator, avoiding any sequential inversions.

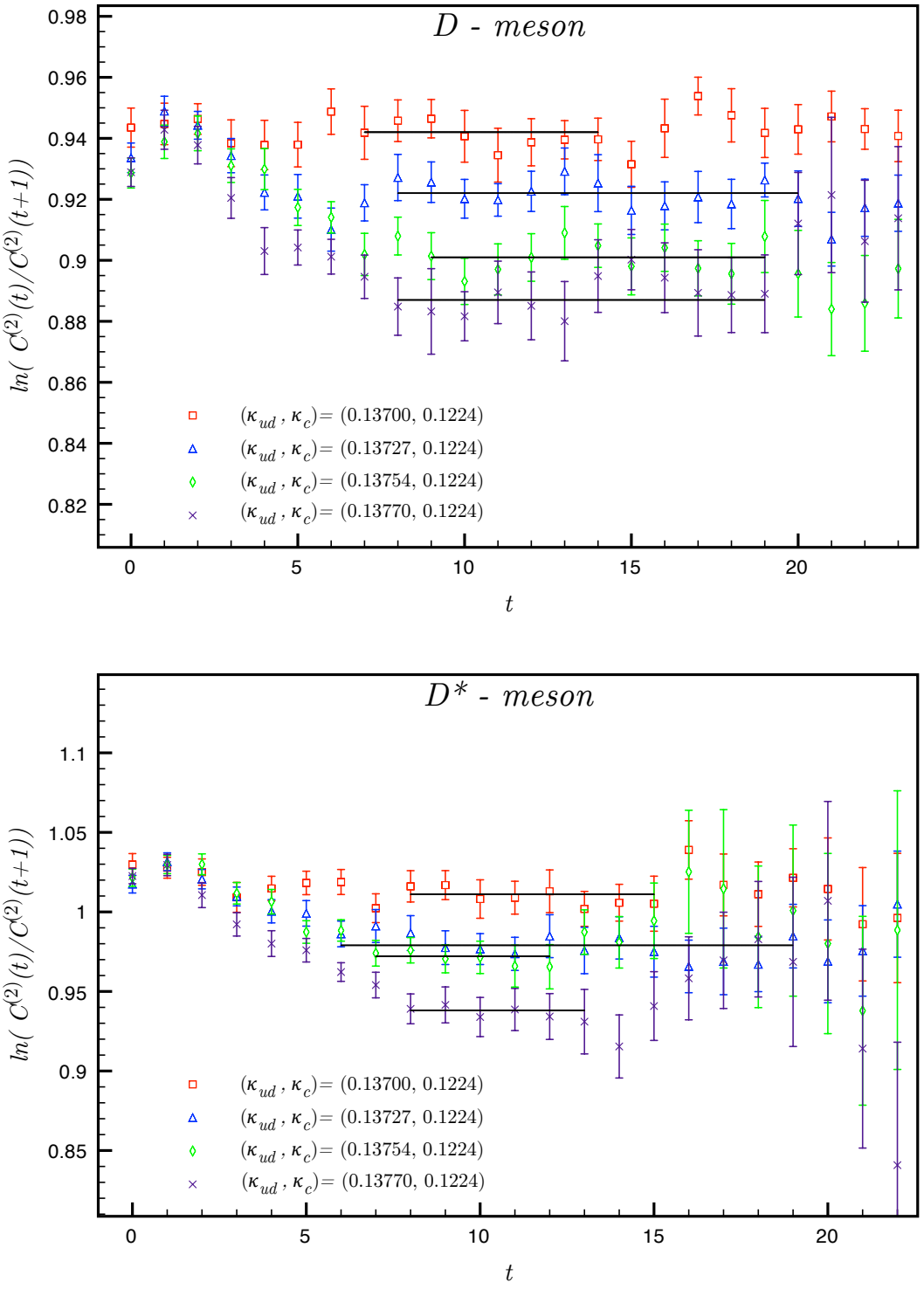

Figure 4.1: Effective mass plots. Black horizontal lines indicate the fit regions.

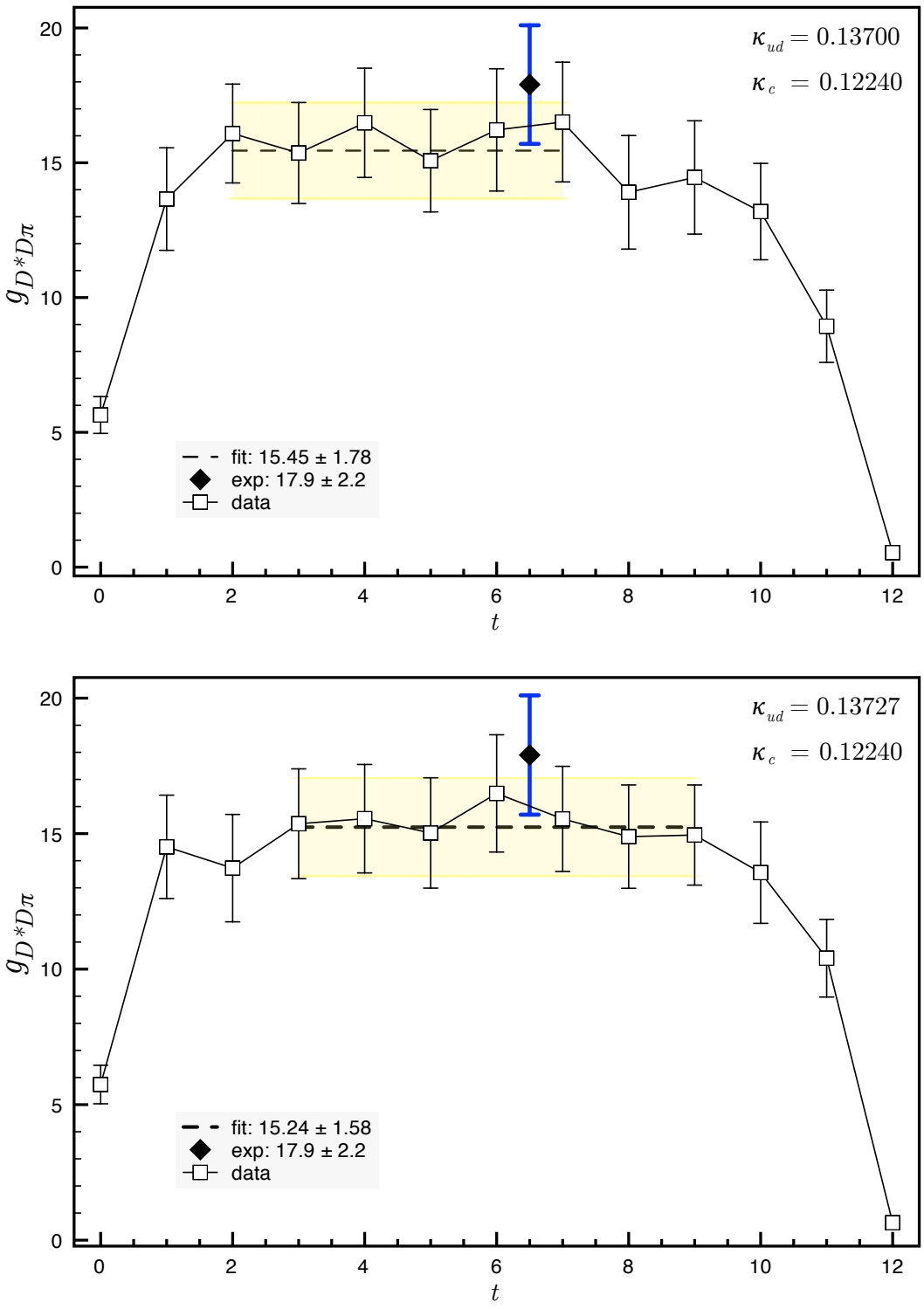

Figure 4.2: Fit regions for $g_{D^*D\pi}$ with error bands. Plots are given for $\kappa_{ud} = 0.13700,\ 0.13727$.

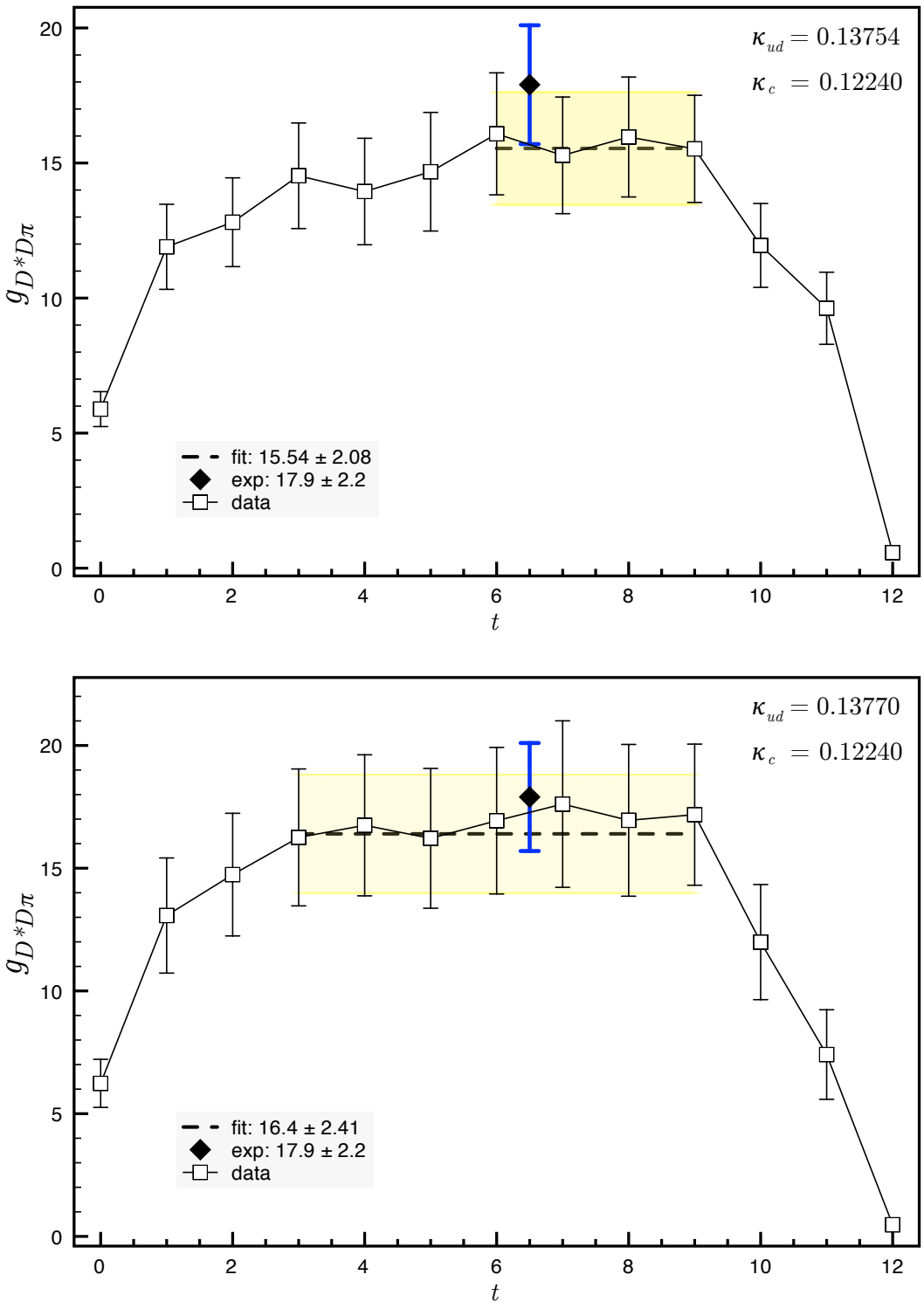

Figure 4.3: Fit regions for $g_{D^*D\pi}$ with error bands. Plots are given for $\kappa_{ud} = 0.13754,\ 0.13770$.

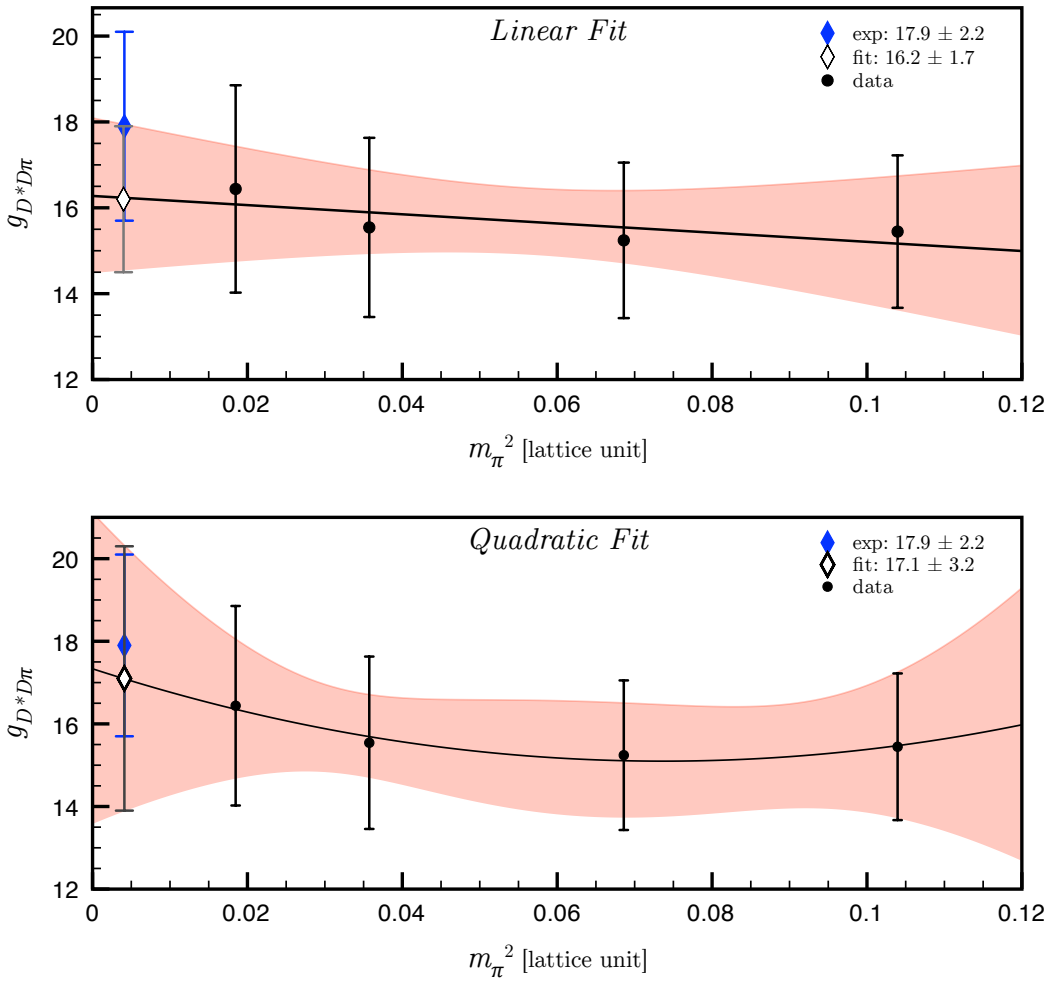

Figure 4.4: $g_{D^*D\pi}$ as a function of m_π^2 in lattice units. The black data points are simulated on configurations with $\kappa_{ud} = (0.13700,\ 0.13727,\ 0.13754,\ 0.13770)$ corresponding to $m_\pi = (700,\ 570,\ 410,\ 300)$MeV. The blue point is the experimental value.